

tag: sPH-CONF-COLDQCD-2025-02

version: 1.0

**DOI:** unspecified **date:** October 19, 2025

### sPHENIX Conference Note

Inclusive jet transverse single spin asymmetries in transversely polarized proton-proton collisions at  $\sqrt{s}=200$  GeV

sPHENIX Collaboration

#### Abstract

We have measured transverse single-spin asymmetries as a function of jet transverse momentum for jet production in the 2024 p+p data-taking period at RHIC, using the sPHENIX detector. The jets were reconstructed from electromagnetic and hadronic calorimeter towers with the anti- $k_T$  algorithm with jet radius of 0.4 and obtained from an estimated luminosity of approximately  $42\,\mathrm{pb}^{-1}$ . The events were selected using calorimeter jet triggers of a minimum energy of 8 GeV, in coincidence with a minimum bias trigger. The results have been fully unfolded for detector effects. The resulting asymmetries are extracted over a transverse momentum range of 10 to 50 GeV and are consistent with zero at both forward and backward rapidities. These asymmetries will help to further constrain the initial-state spin-orbit effects that are related to the quark and gluon Sivers functions.



#### 1 Introduction

The study of transverse single-spin asymmetries (TSSAs) in high-energy polarized proton-proton (p+p) collisions provides critical insight into the inner structure of the proton and the dynamics of Quantum Chromodynamics (QCD). These asymmetries are defined as the left-right imbalance in particle production relative to the transverse spin direction of the incoming proton.

Historically, large TSSAs have been observed for hadrons produced in the forward direction at various energies [1-5], a phenomenon not adequately explained by the standard collinear leadingtwist framework in perturbative QCD. As a result, more sophisticated approaches, such as the transverse momentum dependent (TMD) framework, have been developed to account for these effects. Transverse spin asymmetries are described by convolutions of explicitly transverse momentum dependent parton distribution and fragmentation functions (FFs) that correlate either the proton spin and parton transverse momentum (Sivers effect [6]), or the quark transversity distribution [7] with a spin-dependent fragmentation function (Collins effect [8]). In this framework, two scales are explicitly required to describe these effects, a large scale such as the momentum transfer Q in semi-inclusive deep inelastic scattering (SIDIS) or a large transverse momentum  $(p_T)$  in hadronic collisions and a smaller scale such as the hadron transverse momentum in SIDIS. However, for inclusive measurements in hadronic collisions, one often observes only one large scale, which is typically the transverse momentum of the detected final-state particle or jet. Therefore, a second formalism was developed that tries to explain the transverse spin asymmetries in hadronic collisions based on a collinear higher twist formalism where the effects are generated from quark-gluon-quark or tri-gluon correlations in the initial [9, 10] or final state [11].

These two formalisms have since been found to be related via moments over the explicit transverse momentum dependence of the TMD distribution or fragmentation functions [12], such that in the initial state, the quark-gluon-quark correlators and the tri-gluon correlators are related to the quark and gluon Sivers functions, respectively. Similarly, in the final state the quark-gluon-quark fragmentation correlator can be related to the Collins FF. The large forward single spin asymmetries have been seen for charged and neutral hadrons where both initial state and final state effects can contribute, and a recent global analysis found that final-state contributions are likely dominating [13].

Inclusive jet production is a powerful probe in this context because jets originate from hard parton scatterings and retain information about the initial-state partonic interactions. Since inclusive jets are not biased by FFs, their asymmetries are expected to be sensitive mostly to initial-state effects. Measuring transverse single-spin asymmetries  $A_{\rm N}$  for inclusive jets allows us to test theoretical predictions and better understand the role of parton-gluon correlations in the proton. The STAR collaboration has reported the inclusive jet asymmetry using charged tracks and only the electromagnetic calorimeter for the energy measurement in the midrapidity region [14–16].

In this analysis, we use data collected with the sPHENIX detector at the Relativistic Heavy-Ion Collider (RHIC) [17] during the 2024 transversely polarized proton-proton run at a center-of-mass energy of  $\sqrt{s} = 200\,\text{GeV}$ . Jets are reconstructed using both electromagnetic and hadronic calorimeters at central rapidity. We extracted the  $A_{\rm N}$  for inclusive jets using two methods, the relative luminosity method and the geometric mean (square root) method, to be described in section 4. The measurements are performed as a function of jet  $p_{\rm T}$  for both beams separately, before combining them.



### 2 sPHENIX

The sPHENIX detector [18] is a new detector at RHIC designed to measure jet and heavy-flavor probes of the quark-gluon plasma created in Au+Au collisions at RHIC and to study cold nuclear matter and spin effects in polarized p + p collisions. A precision tracking system enables measurements of heavy-flavor and jet-substructure observables while the electromagnetic and hadronic calorimeter system is crucial for measuring the energy of jets and identifying direct photons and electrons. sPHENIX consists of the following subsystems [18]: the MAPS-based Vertex Detector (MVTX); the INTermediate Tracker (INTT) [19, 20]; the Time Projection Chamber (TPC) [21]; the Time Projection Chamber Outer Tracker (TPOT) [22]; the Electromagnetic Calorimeter (EMCAL) [23,24]; the Inner Hadronic Calorimeter (IHCAL) [24]; the 1.4 T superconducting solenoid magnet [25] and the Outer Hadronic Calorimeter (OHCAL) [24]. Except for the TPOT, all detectors have full azimuthal coverage and span  $|\eta| < 1.1$  in pseudorapidity. sPHENIX also includes several forward detectors, namely the Minimum Bias Detectors (MBD), the sPHENIX Event Plane Detectors (sEPD), and the Zero Degree Calorimeters (ZDC), which include the Shower Maximum Detector (SMD). sPHENIX began its commissioning process in RHIC Run-2023 with Au+Au collisions. During RHIC Run-2024, sPHENIX collected a large sample of transversely polarized p + p collisions at  $\sqrt{s} = 200 \,\mathrm{GeV}$ , alongside a smaller sample of Au+Au data to complete its commissioning phase in that collision system.

### 3 Data and event selection

The data were obtained during the 2024 RHIC running period, where transversely polarized protons at a center-of-mass energy of  $\sqrt{s} = 200\,\mathrm{GeV}$  were collided with average transverse polarizations of 52 and 53%, for the two beams, respectively. A total of  $42\,\mathrm{pb}^{-1}$  has been considered for this analysis in the vertex range, corresponding to roughly 40% of the total accumulated data with the Calorimetry triggers. For this analysis, events were selected if a calorimeter-based jet trigger exceeded a threshold of 8 GeV in a sliding window and where the reconstructed collision vertex z position, as obtained by the MBD, was within 60 cm of the nominal interaction point of  $z=0\,\mathrm{cm}$ .

Jets were reconstructed using towers in EMCAL, IHCAL, and OHCAL, using an anti- $k_T$  algorithm [26] with radius R=0.4. To avoid jets created by beam-related backgrounds, such as muons traversing the HCal scintillator and leaving large amounts of scintillation light, jets whose energy fraction from one of the calorimeters exceeded 90 % of the total energy, less than 10 % for the EMCAL and OHCAL, or less than 0 % for the IHCAL, were discarded. The Calorimeters were calibrated following the procedure described in [27]. To avoid biases at the edges of the acceptance, only jets with pseudorapidities of  $|\eta| < 0.7$  were considered, where all jet constituents should be within the sPHENIX acceptance of  $|\eta| < 1.1$ .

The jet energy scale (JES), defined as the mean of the distribution of the ratio of reconstructed to truth jet  $p_{\rm T}$ , was corrected by using full PYTHIA8 Monte-Carlo (MC) events obtained with the Detroit tune [28] and reconstructed with a GEANT4-based [29] simulation of the sPHENIX detector. We used a MC dataset constructed by merging sub-datasets generated under different conditions: events containing an initial hard interaction with transverse momenta of 10, 20, 30 and 50 GeV, as well as MC minimum-bias events, in order to secure sufficient statistics over a wide  $p_{\rm T}$  range. The



jet energy correction is momentum dependent and slightly decreases with increasing reconstructed transverse momentum. The jet energy scale and resolutions (JER), defined analogously to the JES but using the standard deviation instead of the mean, are displayed in Fig. 1 as a function of the true jet transverse momentum. After the jet energy correction, the corresponding corrected jet energy scale is also shown in Fig. 1 and is consistent with unity over the whole momentum range of interest. Jets in the data were corrected using this energy scale. A 6% variation in the measured asymmetries, due to uncertainty in the jet energy scale, was assigned as a systematic uncertainty. The uncertainty on the jet energy scale was based on calorimeter calibrations using neutral pions and minimum ionizing particles, along with an uncertainty component, which we take from test beam data of the calorimeter system.

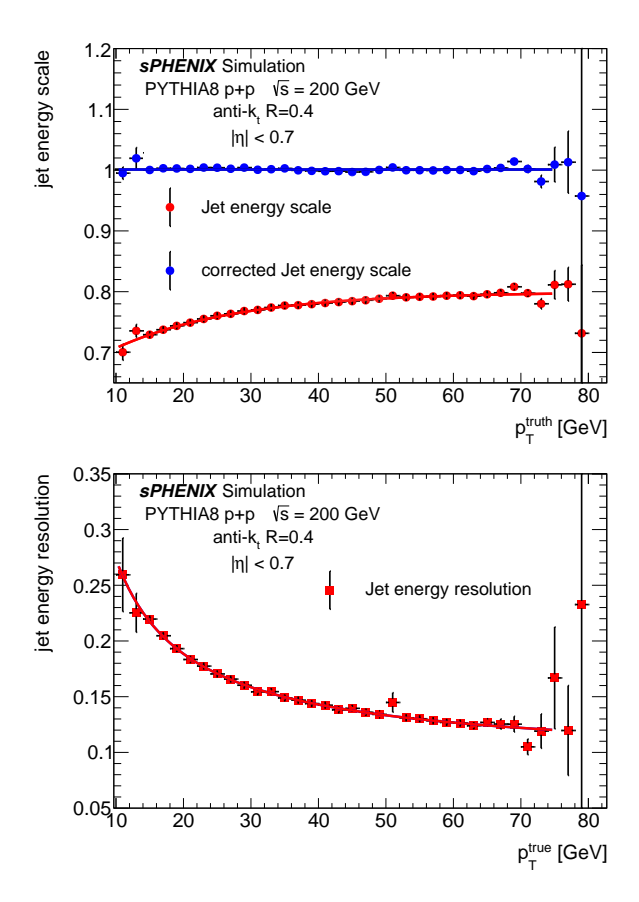


**Figure 1:** Top figure: Jet energy scale as a function of the true jet transverse momentum before (red points) and after (blue points) applying the jet energy correction. The exponential fit to the jet energy scale and a constant fit to the corrected jet energy scale are displayed as red and blue lines, respectively. Bottom figure: Jet energy resolution as a function of the true jet transverse momentum. A power law fit to the jet energy resolution is displayed as red line.

While the jet energy scale correction calibrates the reconstructed jet momenta, it does not correct for the smearing of the momenta. This was therefore performed using an iterative Bayesian unfolding scheme [30] provided by the ROOT package RooUnfold [31]. Since spin asymmetries are not included in generators and unfolding, the unfolding was performed on the raw yields in a two-dimensional binning in transverse momentum and azimuthal angle, for each spin state, pseudorapidity, and beam, separately, and the asymmetries were evaluated after unfolding. The response matrices in the



azimuthal angles are nearly diagonal, given the relatively coarse binning, but in order to calculate azimuthal modulations, they need to be included in the unfolding. The jet energy resolution is also shown in Fig. 1. Previously, the sPHENIX di-jet studies have shown [32] that the MC-based jet energy resolution is underestimated by an amount of  $8\pm3\,\%$  in quadrature compared to existing results. Consequently, when constructing a response matrix for unfolding, reconstructed jet  $p_{\rm T}$  was smeared by this additional factor and varied within its uncertainties to create a more realistic response matrix. Three iterations of the Bayesian unfolding were taken as the central value, while differences with two and four iterations were assigned as systematic uncertainties. Variations from alternative unfolding methods—including a one-dimensional unfolding in azimuthal slices and an unfolding using combined transverse momentum and azimuthal bin indices—are assigned as systematic uncertainties. The closure of the unfolding procedure was tested in simulation and shows that the true kinematic distributions can be reconstructed well. Also the closure of artificially introduced asymmetries has been successfully tested.

### 4 Asymmetry extraction

The relative luminosity formula defined by Eq. 1 is a direct representation of a left-right asymmetry by calculating the count rate differences:

$$A(\phi) = \frac{N^{\uparrow}(\phi) - RN^{\downarrow}(\phi)}{N^{\uparrow}(\phi) + RN^{\downarrow}(\phi)},\tag{1}$$

here,  $R = L^{\uparrow}/L^{\downarrow}$  is the relative luminosity between spin-up and spin-down bunch crossings where the azimuthal angle  $\phi$  runs over the whole  $2\pi$  region. The run-by-run polarization and the relative luminosity are shown in Fig. 2. The two-peak structure in the relative luminosity distributions arises from the difference between the numbers of positively and negatively polarized bunches, since the total number of bunches is odd. The sine modulation of this asymmetry is then related to the raw transverse single-spin asymmetry  $\epsilon_N$ :

$$A(\phi) = \epsilon_{\rm N} \sin(\phi),\tag{2}$$

where the final transverse single spin asymmetry  $A_{\rm N}$  needs to be corrected for the polarization P of the polarized beam:

$$A_{\rm N} = \frac{1}{P} \epsilon_{\rm N}.\tag{3}$$

The relative luminosity method is able to obtain asymmetries even if not the full azimuthal acceptance is available (although corrections would be required), but it requires good knowledge of the accumulated luminosities of both spin states.

The square root formula or geometric formula defined in Eq. 4 is the most trusted formula for estimating  $A_{\rm N}$  since it eliminates both luminosity and most acceptance effects by combining the yields of opposite angles:

$$A(\phi) = \frac{\sqrt{N^{\uparrow}(\phi)N^{\downarrow}(\phi+\pi)} - \sqrt{N^{\downarrow}(\phi)N^{\uparrow}(\phi+\pi)}}{\sqrt{N^{\uparrow}(\phi)N^{\downarrow}(\phi+\pi)} + \sqrt{N^{\downarrow}(\phi)N^{\uparrow}(\phi+\pi)}}.$$
 (4)



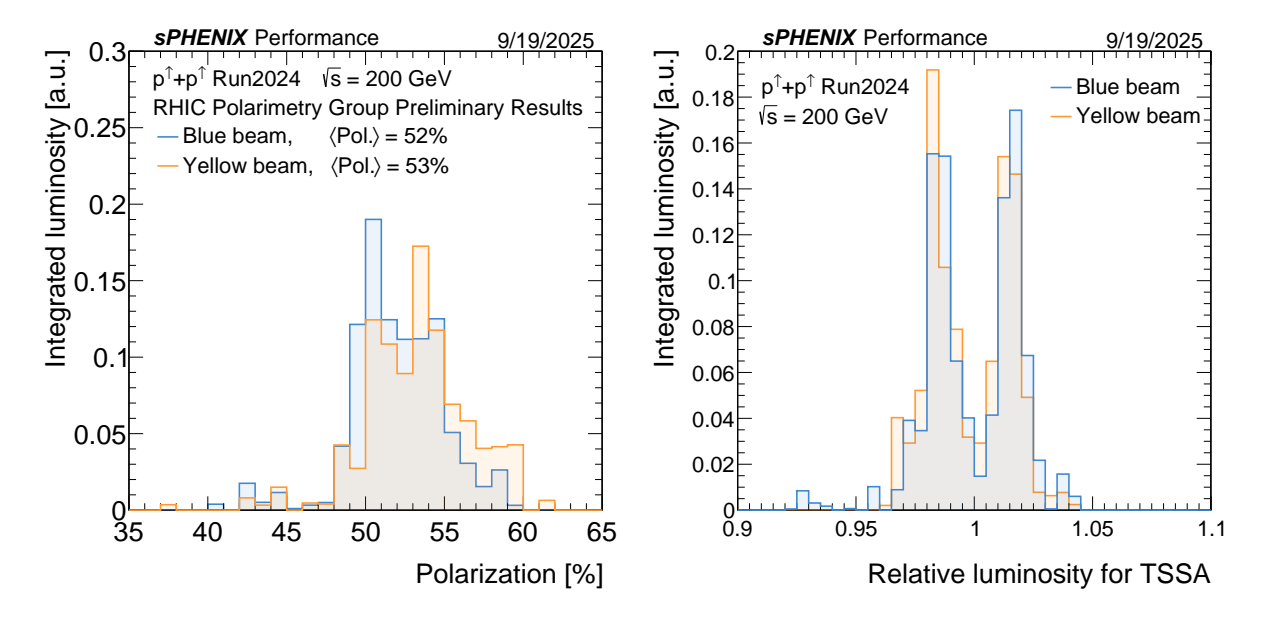


**Figure 2:** Left: Run-by-run polarization for each beam weighted by the luminosity of each run. Right: Run-by-run relative luminosity for each beam weighted by the luminosity of each run.

In this method, a nearly symmetric azimuthal acceptance is required as opposite angles get combined. Consequently, the azimuthal angle runs only over a region of  $\pi$ .

In both methods, the raw asymmetries  $\epsilon_{\rm N}$  were then obtained by fitting the raw azimuthal asymmetries with a sine modulation that can have optionally a constant offset (that particularly would account for incorrect relative luminosities) and a phase present (that accounts for a nonzero angle of the nominal transverse spin orientation). The latter has been found to be consistent with zero by the local polarimeter throughout the sPHENIX p+p running period, but the inclusion/omission of both terms in the fits have been studied. No significant differences for the extracted modulations were found.

# 5 Systematic studies

To obtain the systematic uncertainty, variations from the nominal analyses were applied one at a time, and the whole analysis chain was repeated with the given source.

From the unfolding, three uncertainties were considered. The first one is due to the variation in the number of iterations used in the unfolding. The second originates from the variation using different unfolding methods (two-dimensional vs. one-dimensional unfolding in azimuthal angular slices and one-dimensional unfolding using transverse momentum and azimuthal bin indices). The third stems from the variation of the jet energy resolution in the unfolding. The systematic uncertainties were assigned based on the differences in the resulting asymmetries. Additionally, the jet energy scale itself was varied by 6% and was also assigned as a systematic uncertainty.

Apart from the uncertainties on the unfolding, jet energy scale and resolution, various other systematic tests were performed. The 2024 proton-proton collision data were taken in two distinct



running modes, where the crossing angle between the beams was either zero or 1.5 mrad. No deviations between the two running conditions were seen, and therefore, no additional systematic uncertainties were assigned. Also, the dependence on the longitudinal position of the collision vertex, the polar angular region, and the jet radius were tested. Here, the resulting asymmetries using different selection criteria were used without finding significant deviations between them.

Another test was performed by randomizing the spin orientations of each bunch in each fill and extracting the asymmetries which were expected to be zero and have a width consistent with the extracted statistical uncertainties if no hidden systematic effects are present. The distributions showed no deviations from the expected widths and means, and consequently, no systematic uncertainty was assigned to it. Lastly, the two asymmetry extraction methods mentioned above were compared and found to be consistent with each other. Since both beams were polarized at RHIC, one can obtain two statistically independent measurements for each beam, respectively, while averaging over the polarization of the other beam. After confirming their consistency, these two results have been combined by taking their weighted average.

The overall systematic uncertainties have been obtained from the individual sources mentioned above by adding each contribution in quadrature. Their individual and total contributions are displayed relative to the statistical uncertainties as a function of  $p_{\rm T}$  in Fig. 3. As can be seen, the measurements are generally limited by statistical uncertainties, but particularly the variation of the jet energy scale can be significant as well.

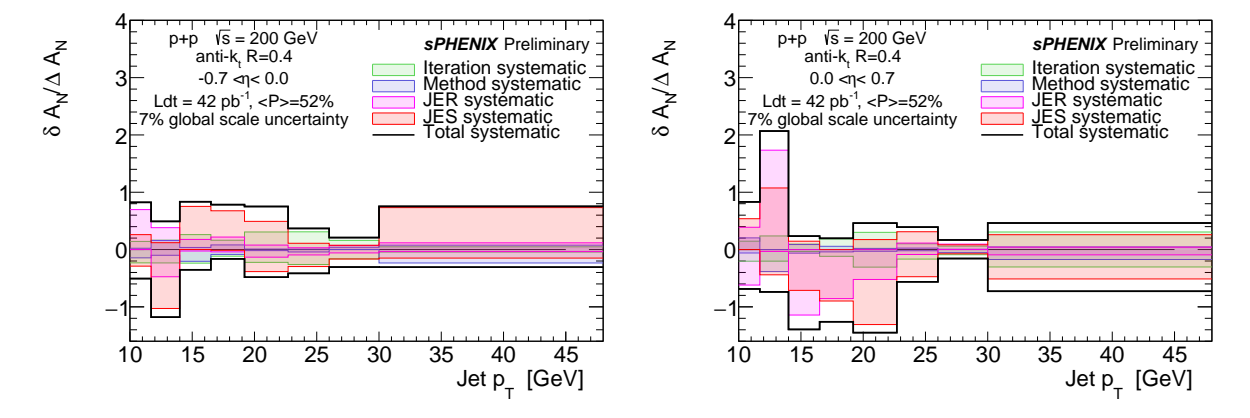


**Figure 3:** Systematics budget for the various individual and total systematic upper and lower uncertainties relative to the statistical uncertainties as a function of the transverse momentum of the jet. The left figure displays the uncertainties for the backward region, while the right figure shows those of the forward region.

### 6 Results

The resulting asymmetries are shown in Fig. 4 for the forward- and backward- going jets, corresponding to  $0 < \eta < 0.7$  and  $-0.7 < \eta < 0$  relative to the polarized proton beam, respectively. The blue boxes represent the systematic uncertainty, and the vertical bars represent the statistical uncertainty. It can be seen that they are consistent with zero and also agree with similar measurements that have been performed by STAR [16], which have roughly similar rapidity coverage and use a jet radius of



0.6. Only the asymmetry results above 10 GeV have been made available, but further studies are expected to extend this range to lower transverse momenta. We also expect to use a larger dataset from the p + p run as calibrations and data processing progresses.

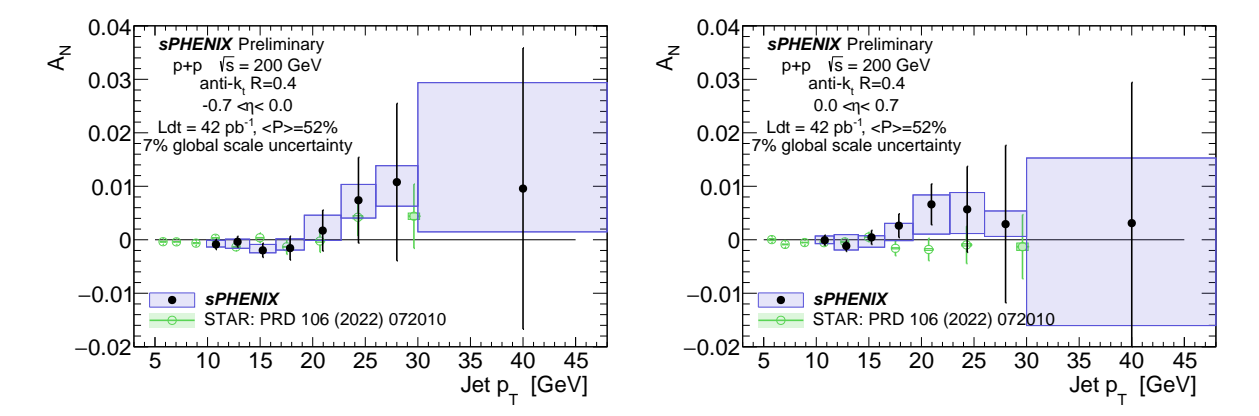


**Figure 4:** Final transverse single spin asymmetries as a function of the jet transverse momentum in the forward and backward regions (full, black symbols), compared to a recent STAR publication of similar observables using charged particles and electromagnetic calorimetry with a radius of 0.6 (dark-green open circles). The left figure displays the asymmetries for the backward region while the right figure shows those of the forward region.

## 7 Summary

We have presented preliminary inclusive jet transverse single spin asymmetries in transversely polarized p + p collisions at central rapidities using a data set of about  $42 \,\mathrm{pb}^{-1}$ . The asymmetries are consistent with zero and also agree with the previous measurement by the STAR collaboration within uncertainties.

### References

- [1] D. L. Adams et al. Comparison of spin asymmetries and cross-sections in  $\pi^0$  production by 200-GeV polarized anti-protons and protons. *Phys. Lett. B*, 261:201–206, 1991. doi: 10.1016/0370-2693(91)91351-U. 1
- [2] D. L. Adams et al. Analyzing power in inclusive  $\pi^+$  and  $\pi^-$  production at high  $\chi_F$  with a 200 GeV polarized proton beam. *Phys. Lett. B*, 264:462–466, 1991. doi:10.1016/0370-2693(91) 90378-4. 1
- [3] J. H. Lee and F. Videbaek. Single spin asymmetries of identified hadrons in polarized p + p at  $\sqrt{s} = 62.4$  and 200 GeV. AIP Conf. Proc., 915(1):533-538, 2007. doi:10.1063/1.2750837. 1
- [4] J. Adams et al. Cross-sections and transverse single spin asymmetries in forward neutral pion production from proton collisions at  $\sqrt{s} = 200$  GeV. *Phys. Rev. Lett.*, 92:171801, 2004. arXiv:hep-ex/0310058, doi:10.1103/PhysRevLett.92.171801. 1



- [5] A. Adare et al. Measurement of transverse-single-spin asymmetries for midrapidity and forward-rapidity production of hadrons in polarized p+p collisions at  $\sqrt{s}$  =200 and 62.4 GeV. *Phys. Rev. D*, 90(1):012006, 2014. arXiv:1312.1995, doi:10.1103/PhysRevD.90.012006. 1
- [6] Dennis W. Sivers. Single spin production asymmetries from the hard scattering of point-like constituents. *Phys. Rev. D*, 41:83, 1990. doi:10.1103/PhysRevD.41.83. 1
- [7] John P. Ralston and Davison E. Soper. Production of dimuons from high-energy polarized proton proton collisions. *Nucl. Phys. B*, 152:109, 1979. doi:10.1016/0550-3213(79)90082-8.
- [8] John C. Collins. Fragmentation of transversely polarized quarks probed in transverse momentum distributions. *Nucl. Phys. B*, 396:161–182, 1993. arXiv:hep-ph/9208213, doi:10.1016/0550-3213(93)90262-N. 1
- [9] A. Efremov, V. Korotkiian, and O. Teryaev. The twist three single spin asymmetries of pion production. *Phys. Lett. B*, 348:577–581, 1995. doi:10.1016/0370-2693(95)00123-3. 1
- [10] Jian-wei Qiu and George F. Sterman. Single transverse spin asymmetries in hadronic pion production. *Phys. Rev. D*, 59:014004, 1999. arXiv:hep-ph/9806356, doi:10.1103/PhysRevD. 59.014004. 1
- [11] Y. Kanazawa and Yuji Koike. Estimate of a chiral odd contribution to single transverse spin asymmetry in hadronic pion production. *Phys. Lett. B*, 490:99–105, 2000. arXiv:hep-ph/0007272, doi:10.1016/S0370-2693(00)00969-2. 1
- [12] J. Collins et al. Relating transverse momentum dependent and collinear factorization theorems in a generalized formalism. *Phys. Rev. D*, 94(3):034014, 2016. arXiv:1605.00671, doi: 10.1103/PhysRevD.94.034014. 1
- [13] Justin Cammarota et al. Origin of single transverse-spin asymmetries in high-energy collisions. Phys. Rev. D, 102(5):054002, 2020. arXiv:2002.08384, doi:10.1103/PhysRevD.102.054002.
- [14] L. Adamczyk et al. Azimuthal transverse single-spin asymmetries of inclusive jets and charged pions within jets from polarized-proton collisions at  $\sqrt{s}=500\,$  GeV. Phys. Rev. D, 97:032004, Feb 2018. URL: https://link.aps.org/doi/10.1103/PhysRevD.97.032004, doi:10.1103/PhysRevD.97.032004. 1
- [15] J. Adam et al. Measurement of transverse single-spin asymmetries of  $\pi^0$  and electromagnetic jets at forward rapidity in 200 and 500 GeV transversely polarized proton-proton collisions. *Phys. Rev. D*, 103:092009, May 2021. URL: https://link.aps.org/doi/10.1103/PhysRevD. 103.092009, doi:10.1103/PhysRevD.103.092009. 1
- [16] M. S. Abdallah et al. Azimuthal transverse single-spin asymmetries of inclusive jets and identified hadrons within jets from polarized pp collisions at  $\sqrt{s}=200\,$  GeV. Phys.~Rev.~D, 106:072010, Oct 2022. URL: https://link.aps.org/doi/10.1103/PhysRevD.106.072010, doi:10.1103/PhysRevD.106.072010. 1, 6
- [17] M. Harrison, T. Ludlam, and S. Ozaki. RHIC project overview. Nuclear Instruments and Methods in Physics Research Section A: Accelerators, Spectrometers, Detectors and Associated Equipment, 499(2):235-244, 2003. The Relativistic Heavy Ion Collider Project: RHIC and its Detectors. doi:10.1016/S0168-9002(02)01937-X. 1
- [18] sPHENIX collaboration. sphenix technical design report, 2019. URL: https://indico.bnl.gov/event/7081/attachments/25527/38284/sphenix\_tdr\_20190513.pdf. 2



- [19] Y. Akiba et al. The ladder and readout cables of intermediate silicon strip detector for sPHENIX.

  Nuclear Instruments and Methods in Physics Research Section A: Accelerators, Spectrometers,

  Detectors and Associated Equipment, 1082:171020, 2026. doi:10.1016/j.nima.2025.171020.

  2
- [20] C. W. Shih et al. Beam test results of the intermediate silicon tracker for sPHENIX, 2025. URL: https://arxiv.org/abs/2509.00908, arXiv:2509.00908. 2
- [21] Henry T. Klest. A Compact TPC for the sPHENIX Experiment. *J. Phys. Conf. Ser.*, 2374(1):012147, 2022. arXiv:2212.05541, doi:10.1088/1742-6596/2374/1/012147. 2
- [22] S. Aune et al. The sPHENIX Micromegas Outer Tracker. Nuclear Instruments and Methods in Physics Research Section A: Accelerators, Spectrometers, Detectors and Associated Equipment, 1066:169615, 2024. doi:10.1016/j.nima.2024.169615. 2
- [23] C. A. Aidala et al. Design and beam test results for the 2-D projective sphenix electromagnetic calorimeter prototype. *IEEE Transactions on Nuclear Science*, 68(2):173–181, 2021. doi: 10.1109/TNS.2020.3034643. 2
- [24] C. A. Aidala et al. Design and beam test results for the sphenix electromagnetic and hadronic calorimeter prototypes. *IEEE Transactions on Nuclear Science*, 65(12):2901–2919, 2018. doi:10.1109/TNS.2018.2879047. 2
- [25] T.G. O'Connor et al. Design and testing of the 1.5 T superconducting solenoid for the BaBar detector at PEP-II in SLAC. *IEEE Transactions on Applied Superconductivity*, 9(2):847–851, 1999. doi:10.1109/77.783429.
- [26] Matteo Cacciari, Gavin P. Salam, and Gregory Soyez. The anti- $k_t$  jet clustering algorithm. JHEP, 04:063, 2008. arXiv:0802.1189, doi:10.1088/1126-6708/2008/04/063. 3
- [27] M. I. Abdulhamid et al. Measurement of the transverse energy density in Au+Au collisions at sNN=200GeV with the sPHENIX detector. *Phys. Rev. C*, 112(2):024908, 2025. arXiv: 2504.02242, doi:10.1103/h8d5-swg6. 3
- [28] Manny Rosales Aguilar et al. Pythia8 underlying event tune for RHIC energies. *Phys. Rev. D*, 105:016011, Jan 2022. doi:10.1103/PhysRevD.105.016011. 3
- [29] S. Agostinelli et al. Geant4—a simulation toolkit. Nuclear Instruments and Methods in Physics Research Section A: Accelerators, Spectrometers, Detectors and Associated Equipment, 506(3):250-303, 2003. URL: https://www.sciencedirect.com/science/article/pii/S0168900203013688, doi:10.1016/S0168-9002(03)01368-8. 3
- [30] G. D'Agostini. A Multidimensional unfolding method based on Bayes' theorem. Nucl. Instrum. Meth. A, 362:487-498, 1995. doi:10.1016/0168-9002(95)00274-X. 3
- [31] Tim Adye. Unfolding algorithms and tests using RooUnfold. In *PHYSTAT 2011*, pages 313–318, Geneva, 2011. CERN. arXiv:1105.1160, doi:10.5170/CERN-2011-006.313. 3
- [32] sPHENIX Collaboration. Measurement of dijet imbalance  $x_j$  and acoplanarity  $(\delta\phi)$  in p+p collisions at  $\sqrt{s}=200$  GeV with the sphenix detector, 2025. URL: https://www.sphenix.bnl.gov/PublicResults/sPH-CONF-JET-2025-01. 3